A stable criterion for shear-wave-splitting analysis

Xinxiang Li, Arcis Seismic Solutions
Jeff P. Grossman*, Sensor Geophysical Ltd.
Jeff_Grossman@sensorgeo.com

GeoConvention 2012:Vision

Summary

Shear-wave-splitting (SWS) effects for HTI media can be characterized by the travel-time difference between the split fast and slow shear waves, and the azimuth of the fast shear-mode. Recent growth in multicomponent technology has seen development of several methods for analyzing SWS effects using PS converted-wave seismic data. Most of these methods rely on the distribution of reflection energy on the transverse component, which increases with the amount of time-delay. Transverse-component-based methods tend to lose stability at low signal-to-noise ratios when marginal splitting occurs, such as in deeper hydrocarbon targets, which often show subtle time delays due to high shear-wave speeds or thinner layering. More robust methods of SWS analysis are required to reliably detect and estimate such subtle anisotropic features. We propose a radial-component-based method that focuses on the majority of the shear-wave energy no matter how much splitting is involved. Examples from real data show the new method produces better results. Although this method is shown to be very precise, it is subject to the same accuracy caveats as any other method, e.g. differential attenuation and correct receiver-azimuth information. We have quantified a source of error arising from differential attenuation, and developed a robust new method to detect, correct for, and quantify uncertainty in receiver azimuth.

Introduction

Application of SWS analysis to seismic exploration has come a long way over the last two decades. Early efforts naturally focused on shear-wave data that were only available as 2D surface seismic or VSP's (Alford 1986, Harrison 1992). More recent significant developments utilize 3D PS converted-wave surface seismic (Bale et al., 2009, Cary et al., 2010). SWS effects can be characterized by the time delays and polarizations of the fast and slow shear modes (Silver & Chan, 1991). Various algorithms exist to estimate these two attributes. Li (1998) and Bale et al. (2005) use the transverse component to estimate fast/slow shear-wave polarizations, and then estimate time delay via crosscorrelation of the fast and slow components. Gaiser (2006) reorganizes the lateral components of the converted shear data to form two source-azimuth vs .two receiver-azimuth (2Cx2C) data matrices based on source-receiver azimuths and radial and transverse azimuths. Alford rotations are applied to these matrices to estimate the fast/slow polarizations by minimizing energy on the off-diagonal matrix components. Simmons (2009) details a full-scan method using radial and transverse components to estimate both attributes simultaneously. The objective is to minimize energy remaining on the transverse component after splitting effects are removed.

All of these approaches are effectively based on the same principle: determine SWS attributes by minimizing energy on the transverse component. All are able to estimate SWS attributes when the splitting is strong enough to distinguish shear-wave-reflection energy from ambient noise. However, when SWS is weak–which often occurs in deeper HTI formations–transverse-component energy is also weak and can be obscured by noise. For vertically travelling shear waves through an HTI layer in a 1D earth model, the transverse-component amplitude is predicted as (Simmons, 2006)

$$\hat{u}_T(t,\theta,\Delta t) = \left[u_R(t) - u_R(t-\Delta t)\right]\sin\theta\cos\theta, \quad (1)$$

where θ is the angle between the source-receiver and polarization axes, Δt is time delay between fast and slow shear modes, and u_R is the radial-component amplitude just before it reaches the HTI layer. We see from (1) that amplitudes on the transverse component not only change periodically with azimuth, they also depend on the time delay between fast and slow shear modes. When $[u_R(t) - u_R(t-\Delta t)]$ is too small relative to noise, due to small Δt values or weak amplitudes of u_R, fitting of the transverse component to equation (1) is unreliable. Thus, energy polarized in the transverse direction may sometimes be ignored, and imaging using only radial component data may suffice to provide satisfactory results. However, we then lose the opportunity to obtain valuable anisotropic properties of subsurface formations.

More robust methods for SWS analysis are therefore certainly desirable. We propose a method based on optimization of the reflection energy distribution on radial-component traces, and demonstrate this method produces superior results. Although this method is quite precise, it remains subject to the same accuracy caveats as any other: specifically, differential attenuation and correct receiver-azimuth information. We recently addressed the latter issue with a robust new method to detect, correct for, and quantify uncertainty in receiver azimuth (Couzens & Grossman, 2012). We are currently researching the former, and briefly illustrate the potential error arising from differential attenuation.

Radial component maximum stack power method

Following the notation of Simmons (2009), the splitting forward modelling operator can be described as

$$\hat{\mathbf{u}} = \mathbf{R}^{-1}\mathbf{D}\mathbf{R}\mathbf{u_0}, \tag{2}$$

where $\mathbf{u}_0 = (u_R, u_T)$ and $\hat{\mathbf{u}} = (\hat{u}_R, \hat{u}_T)$ are the radial and transverse components of the incident wavefield and the wavefield travelling through an HTI layer, respectively, $\mathbf{R}$ is an operator that rotates from radial-transverse coordinates to fast-slow polarization coordinates, and $\mathbf{D}$ is the time-delay operator. The inverse process of equation (2), namely

$$\mathbf{u}_0 = \mathbf{R}^{-1}\mathbf{D}^{-1}\mathbf{R}\hat{\mathbf{u}}, \tag{3}$$

describes the layer-stripping process. Ideally, with known polarization direction and time delay, process (3) removes the splitting effects of the HTI layer. Different inverse-problem schemes can be formed using (3) to estimate the fast shear polarization and the time delays. Instead of using the objective function of total energy remaining on the transverse component, we propose using the stack power of the layer-stripped radial component, i.e.:

$$P_R = \int_{t_1}^{t_2} \left[\int_{\theta_1}^{\theta_2} u_R \, d\theta \right]^2 dt, \tag{4}$$

where the stacking is over the entire azimuth range. Since ranges for the possible azimuths of the fast shear waves and the time delays are clearly defined in practice, a full scan with appropriate sampling in azimuth and time-shift can efficiently provide a global solution to the nonlinear optimization process.

We have experimented with other objective functions that focus on optimizing the radial component: namely, maximum energy on the radial component, and maximum radial/transverse energy ratio. The power or energy of a trace - the summation of the squared sample amplitudes - is independent of time shifts. Thus, neither trace energy nor ratio of trace energy directly reflects temporal alignment of traces. Alternatively, stack power maximization has proven effective in enhancing temporal alignment (Ronen & Claerbout, 1985). The maximization of the stack power of radial component data inherently maximizes only the coherent portion of the energy, and this is consistent with the goal of producing the best quality image from converted wave data. The coherence (or semblance) of a set of traces is defined as the stack power divided by the total energy of all traces that make up the stack. In our optimization process, the coherence of layer-stripped radial-component traces is computed as a QC attribute that indicates the quality of the data and the reliability of the estimates of splitting attributes.

Examples

A 3C dataset from Alberta is used to test different algorithms for SWS analysis. These include the least-squares method of Bale, et al. (2005), and full-scan methods with different objective functions. All work well if the radial and transverse components have reasonably good SNR and the shear wave model fits the data. However, there are areas where some fail to compensate for the SWS effects through layer stripping. Figure 1 shows limited azimuth stacks (LAS) within a time window at two ACP locations. For both ACP's, the leftmost panel (a) is the input radial LAS, where evident sinusoidal events indicate SWS. Panels (b), (c) and (d) are LAS's after layer-stripping, with anisotropy estimated from full-scan algorithms using objective functions of minimum transverse energy, maximum radial energy, and maximum radial/transverse energy ratio, respectively. LAS panel (e) is from Bale et al.'s least-squares method. Panel (f) is from a full-scan method with objective function of radial stack power. The first is an example where all tested methods work very well, while the second shows that our method, panel (f), works the best in terms of aligning the reflection energy across the entire azimuth range.

Figure 2 shows a map (left) with co-rendered time-delays and orientations estimated from the maximum radial-stack-power method. Both the background color and length of the needles represent time delays, and the needle orientation corresponds to the fast direction. This map is useful for interpretation of subsurface anisotropy caused by regional stress, pore-stress changes, or fractures. As a QC tool, the azimuthal coherency map (right) of the radial component identifies whether the data quality and anisotropy estimates are reliable. This QC map shows our estimates are stable since most of the coherence values are above 80%.

Differential attenuation

Vector diagrams in Figure 3 illustrate HTI polarization-estimation error–for a single source/receiver pair–due to differential attenuation when radial/transverse-energy-optimization SWS analysis methods are applied. The orange vectors ((a)-(c)) represent a radially polarized incident PS wave, together with its lossless projections onto the fast/slow polarization directions after splitting. The green vectors ((a), (b)) represent the differentially attenuated polarizations just after transmission. The vector sums are also displayed for each polarized pair. The black vectors in (b) represent what would be measured in radial/transverse coordinates, and (c) shows the erroneous rotation required to eliminate the transverse energy which is present in (b). This error can be very large under normal circumstances when source/receiver-azimuth distribution is poor, such as in 2D surveys. When azimuth distribution is good, errors come in equal-but-opposite-magnitude pairs, and hence tend to cancel out. Our preliminary observations reveal potential both for improved accuracy and for extracting new information about the HTI layer, including differential Q and layer thickness.

Conclusions

A radial-component-based algorithm for SWS analysis was proposed. Using radial and transverse component data, and a SWS, layer-stripping model the method estimates time delays between fast and slow shear modes and orientation of the fast mode by maximizing stack power on the radial-component data. Tests with different datasets and comparisons with other methods show that the maximum-radial-stack-power method is less sensitive to noise and consistently produces precise SWS attributes. We cited a robust new method to detect, correct for, and quantify uncertainty in receiver azimuth. Finally, we illustrated the potential error arising from differential attenuation.

Acknowledgements

We thank our anonymous client for permission to show example results in this paper. We thank Gulia Popov and Peter Cary for discussions regarding stabilization of the SWS methods. Proofreading of the drafts by our colleagues, Rodney Couzens and Robert Pike, was invaluable and much appreciated.

References

Alford, R. M., 1986, Shear data in the presence of azimuthal anisotropy: Dilley, Texas: SEG, Expanded Abstracts, 476-479.
Bale, R., J. Li and B. Mattocks, 2005, SEG, Robust estimation of fracture directions from 3-D converted-waves: SEG Abstracts, 889-892

Bale, R. et al, 2009, Shear wave splitting applications for fracture analysis and improved imaging: First Break, vol. 27 , no. 9, 73-83.
Cary, P., W., X. Li, G. Popov and C. Zhang, 2010, Shear-wave splitting in compliant rocks, The Leading Edge, 29 , no. 10, 1278-1285.
Couzens, R., and J.P. Grossman, 2012, Automated receiver azimuth detection: presented at Sensor Geophysical Symposium.
Gaiser, J., 2006, Minimization of the 4C Alford data matrix for nonorthogonal PS-wave reflection modes, SEG Exp. Abstracts, 1188-1191.
Harrison, M., 1992, Processing of P-Sv surface-seismic data: PhD Thesis, Univ. of Calgary.
Li, X.-Y., 1998, Fracture detection using P-P and P-S waves in multi-component sea-floor data: SEG Expanded Abstracts, 2056-2059.
Ronen, J.and J. F. Claerbout, 1985, Surface-consistent residual statics estimation by stack-power maximization, Geophysics **50**, 2759-2767.
Simmens, J., 2009, Converted-wave splitting estimation and compensation, Geophysics, **74**, P. D37–D48.
Silver, P.G., and W.W.Chan, 1991, Shear wave splitting and subcontinental mantle deformation: J. of Geoph. Research., **96**, 429-454.

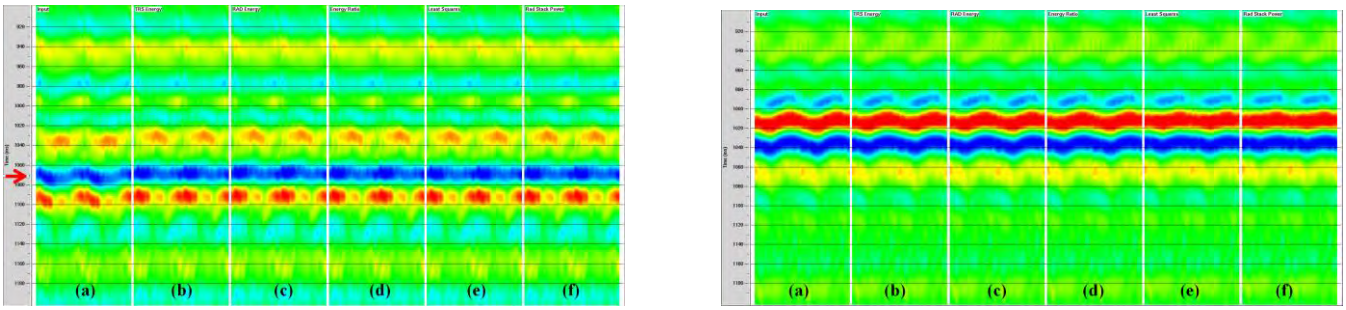

Figure 1: Radial-component limited-azimuth stacks (LAS) formed from supergathering at two ACP locations before ((a)) and after ((b)-(f)) layer stripping using different splitting analysis methods. At the first ACP (left), all methods work well. The layer-stripped radial component traces at different azimuths are well aligned horizontally. At the second location (right), methods (b), (c) and (d) (details in the main text), fail to compensate the SWS effects. The maximum-radial-stack-power method gives the best result, panel (f).

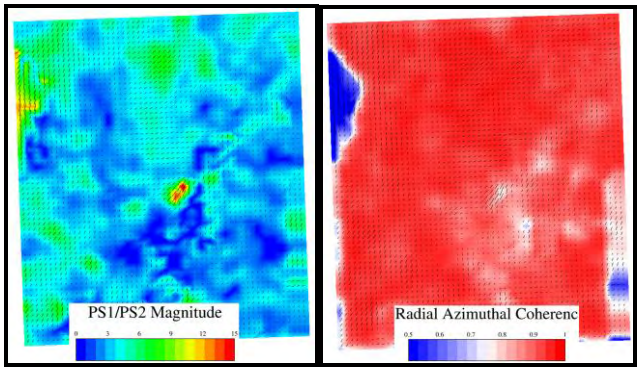

Figure 2: Anisotropy-attribute map (left) from SWS analysis using the maximum-radial-stack-power method; and corresponding radial-component coherence map (right) as a QC for the data quality and the anisotropy estimates.

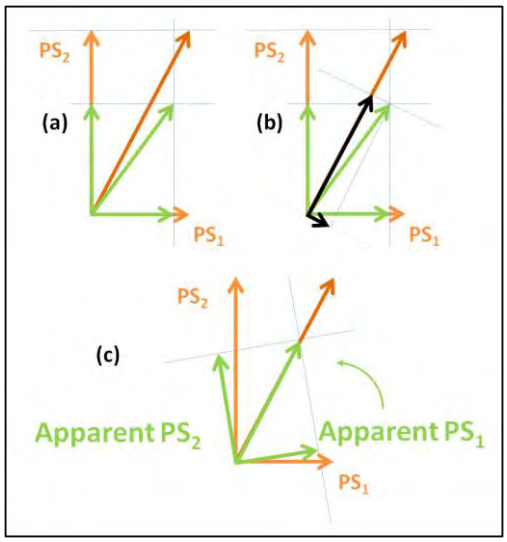

Figure 3. Vector diagrams illustrating HTI polarization-estimation error (for a single shot/ receiver pair) due to differential attenuation when radial/transverse energy-optimization analysis method is applied. Orange vectors ((a)-(c)) denote a radially polarized incident PS wave, and its (lossless) projection onto the fast/slow polarizations after splitting; green vectors ((a), (b)) represent differentially attenuated polarizations just after transmission. The vector sums are also displayed for each polarized pair. The black vectors in (b) represent what would be measured in radial/transverse coordinates, and (c) shows the erroneous rotation required to eliminate the transverse energy.